TABLE 1 Comparison Between Proposed Coupler and Previous Works

	[4]	[5]	[6]	This work
Technology	Branch line	Coupled line	Patch	Patch
Circuit size	0.25λ* 0.25λ	0.25λ* 0.25λ	0.5λ* 0.5λ	0.5λ* 0.5λ
Realizable coupling coefficient (dB)	10	20	10	15
High-frequency applications	No	No	Yes	Yes
Narrow gap	Yes	Yes	No	No
BW (%) (10 dB)	33.3	30	5	29

$$Y_{oe}=\frac{1}{X_{LH1}+\frac{2X_{CH1}X_{LH3}}{2X_{CH1}+X_{LH3}}}+\frac{1}{X_{LV1}}, \tag{9d}$$

where

$$X_{CH1,CV1}=\frac{1}{j\omega C_{CH1,CV1}},$$

$$X_{LH1,LH3,LH4,LV1,LV3,LV4}=j\omega L_{LH1,LH3,LH4,LV1,LV3,LV4}.$$

It can be found that the related parameters are similar to those for the patch coupler with centrally loaded shorting post. But the two parameters L_{LH3} and L_{LV3} for this configuration can be controlled by the positions of shorting posts (P_1 and P_2). Therefore, the range of realizable N can be extended by choosing suitable P_1 and P_2 maintaining the good input/output matching and quadrature phase characteristics.

According to the analysis described in the last section, a 15 dB patch quadrature coupler was designed and fabricated using Rogers RT/Duroid 5870 substrate with dielectric constant ratio 2.33 and thickness $h = 0.787$ mm. The resulting dimensions of the circuit are: $R_1 = 7$ mm, $R_2 = 9$ mm, $R_v = 0.5$ mm, $P_1 = 3$ mm, and $P_2 = 2$ mm. Figure 10 shows the photograph of the designed 15 dB patch quadrature coupler.

Figure 11 shows the simulated and measured frequency responses in terms of S-parameters for the designed 15 dB quadrature patch coupler. Good agreement between simulation and measurement can be observed. The coupling coefficient $|S31|$ is 15 ± 1 dB across the 8–9.7 GHz band. The measured phase difference between the two output ports is $90° \pm 5°$ within the frequency band from 8 to 9.7 GHz. Therefore, the range for the realizable coupling coefficient is extended to 15 dB using the four shorting posts, which cannot be realized using the conventional configuration.

Table 1 summarizes the comparison between the proposed patch quadrature coupler and other structures in the literature. The proposed configuration is found to exhibit the highest fabrication simplicity among the existing configurations for quadrature coupler [1–5], as it eliminates the narrow microstrip line and coupling gap. In addition, the performance of microstrip line based circuits [4,5] becomes poorer with increasing operating frequency; the proposed patch based structure is more suitable for high-frequency applications. Finally, for the first time, the coupling coefficient of patch based quadrature coupler is extended to 15 dB.

4. CONCLUSION

In this article, a method to extend the coupling coefficient range and bandwidth of a patch quadrature coupler is proposed with theoretical analysis for the first time. For demonstration, two patch quadrature couplers have been designed to provide the loose couplings of 10 and 15 dB with wide bandwidths. The validity of proposed approaches had been demonstrated by simulation and measurement.

ACKNOWLEDGMENT

This work was supported by the National Natural Science Foundation of China (NSFC) (No. 61401523) and Science and Technology Program of Guangzhou, China (No. 201510010084).

REFERENCES

1. D. M. Pozar, Microwave Engineering, Wiley, New York, 2005.
2. C.-W. Tang, C.-T. Tseng, and K.-C. Hsu, Design of wide passband microstrip branch-Line couplers with multiple sections, IEEE Trans Compon Packag Manufact Technol 4 (2014), 1222–1227.
3. Y. Wu, Q. Liu, S.-W. Leung, Y. Liu, and Q. Xue, A novel planar impedance-transforming tight-coupling coupler and its applications to microstrip baluns, IEEE Trans Compon Packaging Manuf Technol 4 (2014), 1480–1488.
4. J.-S. Lim, C.-S. Kim, J.-S. Park, D. Ahn, and S. Nam, Design of 10 dB 90° branch line coupler using microstrip line with defected ground structure, Electron Lett 36 (2000), 1784–1785.
5. J. W. Gipprich, A new class of branch-line directional couplers, IEEE MTT-S International Microwave Symposium Digest, Atlanta, GA, 1993, pp. 589–592.
6. S. Y. Zheng, J. H. Deng, Y. M. Pan, and W. S. Chan, Circular sector patch hybrid coupler with arbitrary coupling coefficient and phase difference, IEEE Trans Microwave Theory Tech 61 (2013), 1781–1792.
7. S. Y. Zheng, S. H. Yeung, W. S. Chan, K. F. Man, and S. H. Leung, Size-reduced rectangular patch hybrid coupler using patterned ground plane, IEEE Trans Microwave Theory Tech 57 (2009), 180–188.
8. S. Y. Zheng, W. S. Chan, and K. F. Man, Frequency agile patch element using varactor loaded patterned ground Plane, IEEE Trans Microwave Theory Tech 59 (2011), 619–626.
9. S. Y. Zheng, Y. L. Wu, Y. X, Li, Y. Liu, and Y. L. Long, Dual band hybrid coupler with arbitrary power division ratios over the two bands, IEEE Trans Compon Packaging Manuf Technol 4 (2014), 1347–1358.
10. D. H. Schaubert, F. D. Farrar, A. Sindoris, and S. T. Hayes, Microstrip antennas with frequency agility and polarization diversity, IEEE Trans Antennas Propag AP-29 (1981), 118–123.
11. A. Ali-Khan, W. F. Richards, and S. A. Long, Impedance control of microstrip antennas using reactive loading, IEEE Trans Antennas Propag 37 (1989), 247–251.
12. R. B. Waterhouse, The use of shorting posts to improve the scanning range of probe-fed microstrip patch phased arrays, IEEE Trans Antennas Propag 44 (1996), 302–309.
13. D. R. Jackson, J. T. Williams, A. K. Bhattacharyya, R. L. Smith, S. J. Buchheit, and S. A. Long, Microstrip patch designs that do not excite surface waves, IEEE Trans Antennas Propag 41 (1988), 1501–1509.
14. V. D. Stankovic, B. D. Milovanovic, and J. V. Basta, Analysis of circular-sector-shaped microstrip components using standard electrical CAD programs, *Electrotechnical Conference 1998. MELECON 98, 9th Mediterranean*, Tel-Aviv, Vol. 1, 1998, pp. 246–250.

STRAIN AND CURVATURE-INDEPENDENT TEMPERATURE SENSOR BASED ON AN INTERFEROMETER TAPER FABRICATED WITH A CO_2 LASER

T. J. M. Martins, M. B. Marques, and O. Frazão
Department of Physics and Astronomy, Faculty of Sciences, INESC TEC—Instituto De Engenharia De Sistemas E Computadores, Tecnologia E Ciência, University of Porto, Rua Do Campo Alegre

687, Porto 4169-007, Portugal; Corresponding author: up201000400@fc.up.pt

Received 17 July 2015

ABSTRACT: *An optical fiber interferometer taper fabricated with a CO_2 laser is proposed for strain and curvature-independent temperature measurement. Variations in temperature produce changes in the conditions of the interference between light traveling along the core and cladding and a linear behavior is verified for the relation between the wavelength of the resonant loss peak and temperature, yielding a sensitivity of 110 pm/°C for a range between 25 and 510°C. Both the applied strain and curvature only promote significant changes in the transmitted power, leaving the wavelength of the resonant loss peak approximately constant and rendering this optical sensing device a good strain and curvature-independent temperature sensor.* © 2016 Wiley Periodicals, Inc. Microwave Opt Technol Lett 58:688–691, 2016; View this article online at wileyonlinelibrary.com. DOI 10.1002/mop.29640

Key words: *optical fiber sensor; taper; interferometer*

1. INTRODUCTION

The simultaneous variation of external parameters, such as temperature, curvature, and applied strain, which unavoidably takes place outside a controlled environment, has driven much of the work developed in optical fiber sensing. Several devices have been proposed to overcome this hindrance and more exactly determine the impact of the variation of a single external parameter in the characteristics of the light that interacts with said devices.

Tapers can be used as sensors [1–4]. Two bulge tapers are fabricated in series by a fusion splicer in order to create a Mach Zenhder interferometer [1]. The sensitivities obtained for curvature measurement are -31.821 nm/m^{-1} and -17.051 nm/m^{-1} for small and large range of curvature while the sensitivities for temperature are quite small, being the largest 0.0042 nm/°C, which results in a temperature-independent curvature sensor. A taper was fabricated in a large-mode-area fiber (MOF) with a silica core surrounded by air holes arranged in a hexagonal pattern [2] with a temperature sensitivity of 0.0012 nm/°C. Tapers are fabricated using a butane flame burner to heat the fiber [3]; the largest temperature sensitivity is 0.010 nm/°C and the sensitivity to strain is 0.095 nm/$\mu\varepsilon$, which makes this sensing device an almost temperature-independent strain sensor. A photonic crystal fiber PCF tapered fiber, spliced at both ends to a singlemode fiber (SMF), is produced to obtain an intensity temperature-independent curvature sensor [4], with high sensitivity of 8.35 dBm/m^{-1} in the following range 0.87–1.34 m^{-1}.

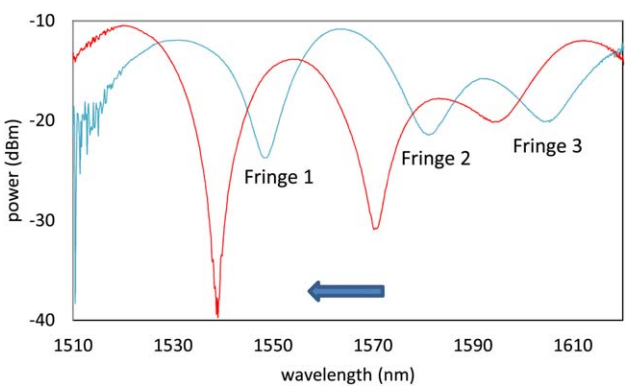

Figure 1 Transmission spectrum evolution for decreasing temperature. The arrow sets the trend for the evolution of the resonant loss peak wavelength for decreasing temperature. [Color figure can be viewed in the online issue, which is available at wileyonlinelibrary.com]

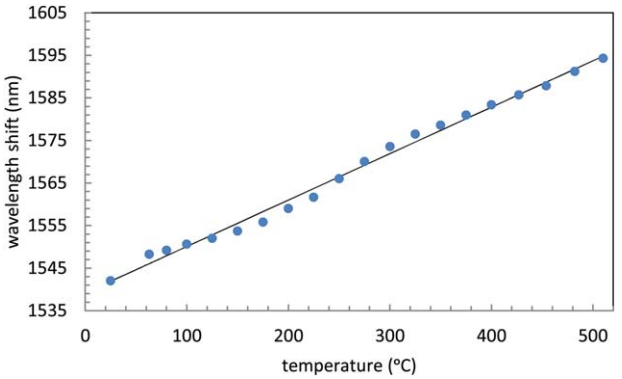

Figure 2 Temperature response of the interferometer taper using the second wavelength peak. Line (linear fit). [Color figure can be viewed in the online issue, which is available at wileyonlinelibrary.com]

CO_2 lasers have also been used to fabricate long-period grating (LPG) structures [5,6]. The reported sensitivities are -7.6 pm/$\mu\varepsilon$ and 3.91 pm/°C, for a LPG inscribed in a PCF [5], which makes the device good for strain sensing since the temperature sensitivity is rather small. A larger temperature sensitivity is also reported and equal to -0.130 nm/°C when the LPG is inscribed in a standard SMF28 fused silica optical fiber [6].

The work presented aims at evaluating the sensitivities of an optical fiber interferometer taper fabricated with a CO_2 laser to temperature, strain, and curvature. The proposed device is interrogated in transmission and the evolution of the fringes of the analyzed spectrum registered for different values of the external parameters. Considering the evolution of the wavelength of the resonant loss peaks λ_m $m = 1,2,3$, a good temperature sensor is obtained, with very small sensitivity to strain and curvature.

2. FABRICATION AND EXPERIMENTAL RESULTS

Taper fabrication is accomplished using an experimental setup including a CO_2 laser and a set of PC controlled motorized stages. The CO_2 laser active medium is excited by an electrical signal with pulse width modulation (PWM) of 25%, corresponding to a laser power of 4.5 W, and a frequency of 10 kHz. The stages parameter values are set so the y-stage and the x-stage have speeds equal to 14 μm/s and 8 μm/s, respectively. The taper length is set equal to 10 mm. The duration of the fabrication process is 1 min and 42 sec. In order to characterize the tapers fabricated using the CO_2 laser as sensors of curvature and strain, the fiber is fixed onto a manually controlled translation stage as well as onto a block placed at a distance $2L$ from the stage. As the distance between the two points where the fiber is fixed changes, so does the curvature of the portion of the fiber between the stage and the block. If this portion of the fiber contains the taper, then it will also experience a change in curvature. The characterization in strain is performed moving the stage up to the point where there is no curvature, and then beyond that point in order to stretch the fiber and increase the applied mechanical stress. The resulting changes in the spectrum of the transmitted light are evaluated using an Optical Spectrum Analyzer (OSA). The broadband light source has a central wavelength of 1,550 nm, with a bandwidth of 100 nm and an average power of -30 dBm (Figure 1).

Light propagating along the core and the cladding has different refractive indices associated. This difference in refractive index Δn can be determined using the wavelength spacing $\Delta\lambda$ between two loss peaks in the transmitted spectrum; in this

case, resorting to the spectrum, $\Delta n \sim 8 \times 10^{-3}$, which means the fabrication process has left the core still with an appreciable diameter and a significant portion of the light still travels along the core even at the tapered region. In this case, the taper presents a similar behavior to a Mach Zenhder configuration.

The experimental setup designed to perform temperature characterization is similar to the one implemented for strain and curvature characterization except for the inclusion of an oven, responsible for controlling the taper temperature. The manually controlled stage was kept in the setup in order to allow for a quick change of the taper curvature making it easier to tune the characteristics of the transmitted spectrum.

2.1. Temperature Measurements

The attention was focused on evaluating how the wavelength of the resonant loss peak λ_m and power of the minima P_m evolve as temperature changes. For the tapers under study, there is a simultaneous variation in both λ_m and P_m, meaning that both the interference conditions as well as interface characteristics, namely the refractive index difference between core and cladding, change during the characterization process. Using the second fringe $m = 2$, located at 1591.22 nm for a temperature equal to 510°C (Figure 2), a good linear behavior is obtained with a sensitivity of 110 pm/°C for a large range of temperatures between 25 and 500°C. As for the intensity variation with temperature, a not so easily discernible trend is obtained, meaning this data is not adequate to be used for calibration purposes. Using the other two fringes, fringe 1, located at 1561.12 nm, and fringe 3, located at 1613.90 nm, linear behaviors are also achieved for the same range of temperatures with similar values for the sensitivities.

2.2. Strain Measurements

The tested taper shows a considerable variation concerning the power P_2 associated to the minima at 1541.30 nm, a value determined for no strain applied to the optical fiber. The wavelength of the resonant loss peak remains approximately the same throughout the entire characterization, with a sensitivity of 1 pm/$\mu\varepsilon$, comprehending values of strain in the range between 0 to 1300 $\mu\varepsilon$ (Figure 3). Such result can be explained by the fact that the applied strain does not change the interference conditions significantly. The refractive index difference Δn between core and cladding remains approximately unchanged as well as the difference in length ΔL light travels along these two portions of the fiber, given the approximate mechanical stiffness. On the other hand, the applied strain might contribute to a reconfiguration of the transition region, making it even smoother which results in lower power losses, leading to an increase in the average transmitted power. The estimated variation in temperature resulting from applied strain is 0.01°C/$\mu\varepsilon$. The maximum deviation from the average of the registered λ_2 is 0.04%.

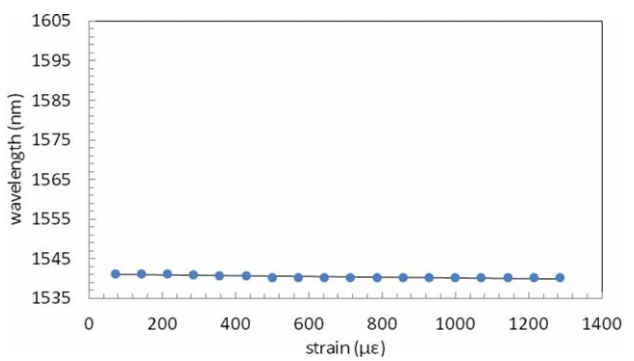

Figure 3 Strain response of the interferometer taper using the first wavelength peak. Line (linear fit). [Color figure can be viewed in the online issue, which is available at wileyonlinelibrary.com]

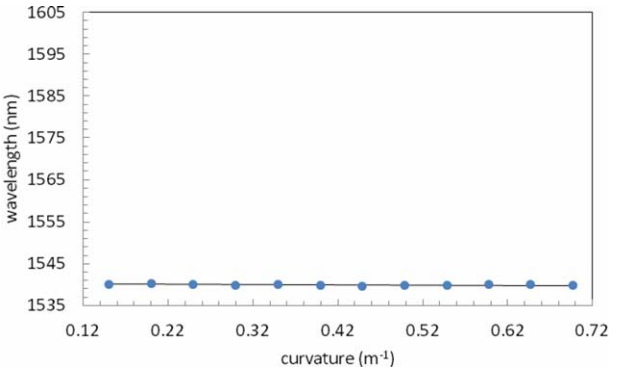

Figure 4 Curvature response of the interferometer taper using the first wavelength peak. Line (linear fit.). [Color figure can be viewed in the online issue, which is available at wileyonlinelibrary.com]

2.3. Curvature Measurements

The calculation of the curvature can be performed in a rather smooth fashion. If the definition of curvature C is taken to be $1/R$, then it can be explicitly written as a function of the easily measured distances L and h (vertical distance between the middle point of the curved fiber and the completely stretched fiber) [7]

$$R^2 = L^2 + (R-h)^2 \iff \frac{1}{R} = \frac{2h}{h^2+L^2} \tag{1}$$

Curvature measurements are performed and, once again, variations in both P_2 and λ_2 are registered. The changes in λ_2 are not very significant in the curvature range between 0.14 and 0.70 m^{-1} (Figure 4). The estimated variation in temperature resulting from applied curvature is 4.55°C/m^{-1}. The maximum deviation from the average of the registered λ_2 is 0.02%.

3. CONCLUSION

The proposed optical device is a good interferometer taper sensor of temperature, if one considers for calibration the curve of wavelength versus temperature, for the temperature range between 25 and 510°C with sensitivity 110 pm/°C. A remarkable result comes up when this taper is characterized in strain, since λ_2 ends up being rather insensitive to changes in applied strain. The same conclusion can be withdrawn after testing the response of the taper in curvature, which renders this device a strain and curvature-independent temperature sensor. The estimated variations in temperature resulting from applied strain and curvature are 0.001°C/$\mu\varepsilon$ and 4.55°C/m^{-1}, respectively. To this outstanding characteristic one can add the fact that the temperature sensitivity is larger than the one verified for many tested devices in literature as well as the large range of temperatures one can cover resorting to this sensor, also benefiting from an easy and quick fabrication process.

ACKNOWLEDGMENTS

This work was financed by FCT—Fundação para a Ciência e Tecnologia (Portuguese Foundation for Science and Technology) and by ERDF (European Regional Development Fund) through: COMPETE Programme (Operational Programme for Competitiveness) within project FCOMP-01-0124-FEDER-037281; ON.2—O Novo Norte (Northern Portugal Regional Operational Programme).

REFERENCES

1. C. Zhang, J. Zhao, C. Miao, Z. Shen, H. Li, and M. Zhang, High-sensitivity all single-mode fiber curvature sensor based on bulge-taper structures modal interference, Opt Commun 336 (2015), 197–201.
2. D. Monzón-Hernández, V.P. Minkovich, and J. Villatoro, High-temperature sensing with tapers made of microstructured optical fiber, IEEE Photon Technol Lett 18 (2006), 511–513.
3. K. Keu and M. Mansuripur, Biconical fiber taper sensors, IEEE Photon Technol Lett 18 (2006), 2239–2241.
4. K. Ni,T. Li, L. Hu, W. Qian, Q. Zhang, and S. Jin, Temperature-independent curvature sensor based on tapered photonic crystal fiber interferometry, Opt Commun 285 (2012), 5148–5150.
5. Y. Wang, L. Xiao, D.N. Wang, and W. Jin, Highly sensitive long-period fiber-grating strain sensor with low temperature sensitivity, Opt Lett 31 (2006), 3414–3416.
6. H. Xuan, W. Jin, and M. Zhang, CO_2 laser induced long period gratings in optical microfibers, Opt Express 17 (2009).
7. C. Gouveia, P.A.S. Jorge, J.M. Baptista, O. Frazão, Temperature-independent curvature sensor using FBG cladding modes based on a core misaligned splice, IEEE Photon Technol Lett 23 (2011), 804–806.

THE EFFECT OF VOID ON CHARACTERISTICS OF LDMOS POWER AMPLIFIER

Mi-Hyun Son,[1] Sooho Bae,[2] Hyuncheol Park,[1] and Hyuck M. Kwon[3]

[1] Department of Electrical Engineering, Korea Advanced Institute of Science and Technology (KAIST), Daejeon, Republic of Korea; Corresponding author: rfamh@kaist.ac.kr

[2] Samsung Electronics Co, Ltd, Suwon, Republic of Korea

[3] Department of Electrical Engineering and Computer Science, Wichita State University, Wichita, Kansas 67260

Received 22 July 2015

ABSTRACT: *The effect of void on characteristics of the laterally diffused metal oxide semiconductor (LDMOS) power amplifier (PA) is analyzed using the thermal and circuit analysis together. Thermal analysis is performed for finding the junction temperature of LDMOS PA as void area changes. Circuit analysis is performed from these results and LDMOS PA libraries. The analysis results show the linearity, gain, and efficiency degradation in the LDMOS PA as a result of the increase in void area. And this simulation methodology can be used for the design of the PA.* © 2016 Wiley Periodicals, Inc. Microwave Opt Technol Lett 58:691–694, 2016; View this article online at wileyonlinelibrary.com. DOI 10.1002/mop.29642

Key words: *void; LDMOS; power amplifier; RRH; linearity*

1. INTRODUCTION

Modern wireless communication networks, such as wideband code division multiple access (WCDMA) and long-term evolution (LTE), make use of complex modulation schemes to maximize data throughput in a limited bandwidth. In general, their resultant communication signals exhibit a high peak-to-average power ratio (PAPR) [1]. Thus, high efficiency and linearity characteristics of power amplifiers (PAs) are required for these WCDMA and LTE base station (BS) applications.

Some microelectronic devices as well as high-power radio frequency (RF) PAs used in BSs typically dissipate non-negligible amounts of heat [2]. Thereby, the junction temperatures of PAs increase during operating conditions in the remote radio head (RRH) of BS [3].

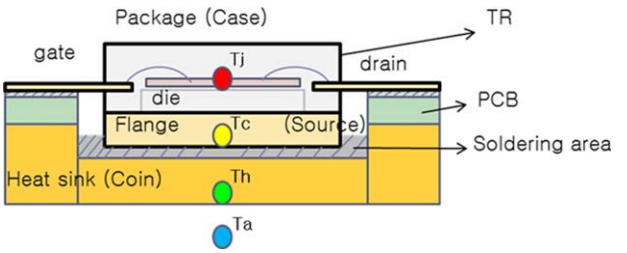

Figure 1 Cross-section view of LDMOS PA. (a) Tj: junction temperature, (b) Tc: case temperature, (c) Th: heat sink temperature, (d) Ta: ambient temperature. [Color figure can be viewed in the online issue, which is available at wileyonlinelibrary.com]

Generally, a heat sink or coin has been used to pull heat from a PA to the outside. But the soldering parts between the heat sink and the PA have not been completely bonded in a practical manufacturing process, and hence a gap, or "void," is inevitable. The voids between a PA transistor and a heat sink can disturb the efficiency of the heat transformation [2].

Previous research results have been reported for the junction temperature of a semiconductor device by using thermal analysis or a self-heating circuit model [4–8]. The relation between the void and the heat dissipation has been researched [9,10]. However, the previous researches of the void are focused on a view point of thermal parameter [11]. PA characteristic with void is rarely reported, especially for WCDMA or LTE BS application.

In this letter, the effect of void on characteristics of the laterally diffused metal oxide semiconductor (LDMOS) PA is analyzed using the thermal and circuit analysis together.

First, this paper presents modeling approaches as to how the thermal effect of the void area changes the junction temperature. Then, thermal analysis is performed on the LDMOS PA using heat-generation devices in RRH by varying the void area. With thermal analysis results, DC and RF characteristics of the LDMOS PA are analyzed for the circuit analysis in terms of linearity, gain, and efficiency of the PA for cases with 0%, 50%, and 75% void areas. Finally, both a WCDMA modulation signal and a CW signal are applied for simulations. Simulation analysis results are compared with the publically available measurement data, and conclusions are made. This is to verify that the simulation analysis is valid and can be used for the design of the PA.

2. STRUCTURE OF LDMOS POWER TRANSISTOR WITH VOID ON PRINTED CIRCUIT BOARD

Figure 1 shows a cross section of the LDMOS power transistor described as follows: gold wire bonds are used to make the connections between the lead and the die; gate and drain side-leads of the transistor are soldered to the printed circuit board (PCB);

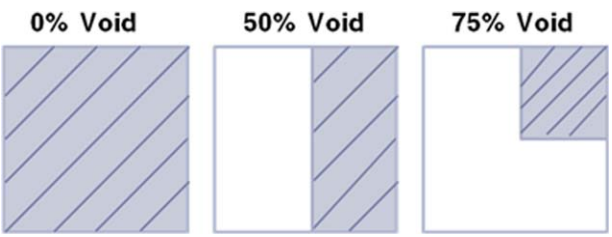

Figure 2 Top view of void area in soldering. [Color figure can be viewed in the online issue, which is available at wileyonlinelibrary.com]